

**Boundary Modifications of the Dissipation
Operators for the Three-dimensional
Euler Equations**

Pelle Olsson and S. Lennart Johnsson

YALEU/DCS/TR-737

September 1989

To appear in the Journal of Scientific Computing

Boundary Modifications of the Dissipation Operators for the Three-dimensional Euler Equations

Pelle Olsson¹

Department of Scientific Computing
Uppsala University
Uppsala, Sweden

and

Department of Computer Science
Yale University
New Haven, CT 06520

S. Lennart Johnsson
Thinking Machines Corp.
245 First Street
Cambridge, MA 02142

and

Departments of Computer Science
and Electrical Engineering
Yale University
New Haven, CT 06520

September 23, 1989

¹This project was partially sponsored by The Swedish Board of Technical Development (STU), reg-no 61008767, by Jacob Letterstedts fond, The Royal Swedish Academy of Sciences, and by the Office of Naval Research under Contract No. N00014-86-K-0310.

Abstract

Explicit methods for the solution of fluid flow problems are of considerable interest in supercomputing. These methods parallelize well. The treatment of the boundaries is of particular interest both with respect to the numeric behavior of the solution, and the computational efficiency. We have solved the three-dimensional Euler equations for a twisted channel using second-order, centered difference operators, and a three stage Runge-Kutta method for the integration. Three different fourth-order dissipation operators were studied for numeric stabilization: one positive definite, [8], one positive semidefinite, [4], and one indefinite. The operators only differ in the treatment of the boundary. For computational efficiency all dissipation operators were designed with a constant bandwidth in matrix representation, with the bandwidth determined by the operator in the interior. The positive definite dissipation operator results in a significant growth in entropy close to the channel walls. The other operators maintain constant entropy.

Several different implementations of the semidefinite operator obtained through factoring of the operator were also studied. We show the difference both in convergence rate and robustness for the different dissipation operators, and the factorizations of the operator due to Eriksson. For the simulations in this study one of the factorizations of the semidefinite operator required 70 - 90% of the number of iterations required by the positive definite operator. The indefinite operator was sensitive to perturbations in the inflow boundary conditions. The simulations were performed on a 8,192 processor Connection Machine system model CM-2. Full processor utilization was achieved, and a performance of 135 Mflops/s in single precision was obtained. A performance of 1.1 Gflops/s for a fully configured system with 65,536 processors was demonstrated.

1 Introduction

Explicit methods are of considerable interest in supercomputing. Supercomputer architectures are parallel architectures. Some of today's supercomputers have thousands to tens of thousands of processors. The next generation supercomputers with a performance of a trillion floating-point operations per second are all expected to have thousands to tens of thousands of processors [6]. Explicit methods parallelize well, but depend critically on the use of artificial viscosity to stabilize the numerical scheme. The treatment of the boundaries is important numerically and computationally. With a lower order difference operator at the boundary, the boundary operator can be designed to contain a subset of the points of the operator in the interior. The complete set of stencils for the interior and the boundary can be represented as a matrix of constant bandwidth. Such a collection of operators results in good load balance and communication efficiency on parallel computers. Several methods for the introduction of artificial viscosity have been proposed, with the one proposed by Eriksson [4] being one of the most common. It is positive semidefinite. We have also included a positive definite [8] and an indefinite operator in our study. We demonstrate how different implementations of the same dissipation operator affect the robustness of an operator. We also demonstrate the importance of a conservative dissipation operator on the flow in a twisted channel with grids of up to 65,536 points. The simulations were carried out on Connection Machine systems, model CM-2. Most of the results were obtained on a 8,192 processor configuration. A performance of 1.1 Gflops/s was demonstrated on a 65,536 processor system. The data parallel implementation is described in [7].

The Euler equations are stated in the next section, in which also the boundary conditions are treated in detail. The artificial viscosity is treated in section 3, and the computational results presented in section 4. Summary and conclusions are given in section 5.

2 The Mathematical Model

2.1 The Interior

Our simulations are based on the conservative formulation of the Euler equations in order to allow for shock capturing. The conservative Euler equations are

$$\frac{\partial \mathbf{q}}{\partial \tau} = \frac{\partial \mathbf{F}}{\partial \xi} + \frac{\partial \mathbf{G}}{\partial \eta} + \frac{\partial \mathbf{H}}{\partial \zeta}, \quad (1)$$

where the variable vector \mathbf{q} is given by

$$\mathbf{q} = |\mathbf{J}|^{-1} \begin{pmatrix} \rho \\ \rho u \\ \rho v \\ \rho w \\ e \end{pmatrix}. \quad (2)$$

The components of the variable vector \mathbf{q} have the following meaning:

- ρ density
- ρu x-component of linear momentum
- ρv y-component of linear momentum
- ρw z-component of linear momentum
- e total energy.

Here τ, ξ, η and ζ denote the variables in the computational domain. The transformation between the computational domain and the physical domain represented by $t, x, y,$ and z is assumed to be continuously differentiable and non-singular:

$$\begin{cases} \tau = t \\ \xi = \xi(t, x, y, z) \\ \eta = \eta(t, x, y, z) \\ \zeta = \zeta(t, x, y, z) \end{cases}.$$

The Jacobian matrix \mathbf{J} is defined by

$$\mathbf{J} = \begin{pmatrix} 1 & 0 & 0 & 0 \\ \xi_t & \xi_x & \xi_y & \xi_z \\ \eta_t & \eta_x & \eta_y & \eta_z \\ \zeta_t & \zeta_x & \zeta_y & \zeta_z \end{pmatrix}. \quad (3)$$

The subscripts denote partial differentiation. The functional determinant of the Jacobian matrix, $|\mathbf{J}|$, corresponds to the reciprocal cell volume:

$$|\mathbf{J}| = \det \mathbf{J} = \det \begin{pmatrix} 1 & 0 & 0 & 0 \\ \xi_t & \xi_x & \xi_y & \xi_z \\ \eta_t & \eta_x & \eta_y & \eta_z \\ \zeta_t & \zeta_x & \zeta_y & \zeta_z \end{pmatrix} = \det \begin{pmatrix} (\nabla \xi)^T \\ (\nabla \eta)^T \\ (\nabla \zeta)^T \end{pmatrix}, \quad (4)$$

where

$$\nabla^T = \left(\frac{\partial}{\partial x} \quad \frac{\partial}{\partial y} \quad \frac{\partial}{\partial z} \right). \quad (5)$$

The flux vectors \mathbf{F} , \mathbf{G} and \mathbf{H} have the following components (inviscid case):

$$\mathbf{F} = -|\mathbf{J}|^{-1} \begin{pmatrix} \rho U \\ \rho u U + p\xi_x \\ \rho v U + p\xi_y \\ \rho w U + p\xi_z \\ (e+p)U - p\xi_t \end{pmatrix} = -U\mathbf{q} - p|\mathbf{J}|^{-1} \begin{pmatrix} 0 \\ \nabla\xi \\ U - \xi_t \end{pmatrix} \quad (6)$$

$$\mathbf{G} = -|\mathbf{J}|^{-1} \begin{pmatrix} \rho V \\ \rho u V + p\eta_x \\ \rho v V + p\eta_y \\ \rho w V + p\eta_z \\ (e+p)V - p\eta_t \end{pmatrix} = -V\mathbf{q} - p|\mathbf{J}|^{-1} \begin{pmatrix} 0 \\ \nabla\eta \\ V - \eta_t \end{pmatrix} \quad (7)$$

$$\mathbf{H} = -|\mathbf{J}|^{-1} \begin{pmatrix} \rho W \\ \rho u W + p\zeta_x \\ \rho v W + p\zeta_y \\ \rho w W + p\zeta_z \\ (e+p)W - p\zeta_t \end{pmatrix} = -W\mathbf{q} - p|\mathbf{J}|^{-1} \begin{pmatrix} 0 \\ \nabla\zeta \\ W - \zeta_t \end{pmatrix}, \quad (8)$$

and U , V and W are the contravariant velocity components:

$$\begin{pmatrix} U \\ V \\ W \end{pmatrix} = \mathbf{J}' \begin{pmatrix} 1 \\ u \\ v \\ w \end{pmatrix}. \quad (9)$$

\mathbf{J}' denotes the 3×4 matrix which is obtained by deleting the first row of \mathbf{J} . In the flux vector expressions, p denotes the pressure, which is related to the total energy according to

$$p = (\gamma - 1)\left(e - \frac{\rho}{2}(u^2 + v^2 + w^2)\right), \quad (10)$$

where γ is the ratio of the specific heats c_p/c_v . We assume that γ is a constant having the value 1.4.

2.2 The Boundary

In deriving the appropriate boundary conditions we consider the linearized Euler equations in non-conservative form for convenience. The non-conservative, or *primitive*, variables are

$$\mathbf{r} = \begin{pmatrix} \rho \\ u \\ v \\ w \\ p \end{pmatrix}. \quad (11)$$

Using equations (2), (10) and (11) it is possible to establish a relationship between \mathbf{q} and \mathbf{r} . For the linearized problem the boundary conditions leading to a well posed problem for

the non-conservative formulation will also lead to a well posed problem for the conservative formulation. By the chain rule equation (1) is transformed into

$$\frac{\partial \mathbf{r}}{\partial \tau} = \mathbf{A} \frac{\partial \mathbf{r}}{\partial \xi} + \mathbf{B} \frac{\partial \mathbf{r}}{\partial \eta} + \mathbf{C} \frac{\partial \mathbf{r}}{\partial \zeta}, \quad (12)$$

where

$$\mathbf{A} = \left(\frac{\partial \mathbf{q}}{\partial \mathbf{r}} \right)^{-1} \frac{\partial \mathbf{F}}{\partial \mathbf{q}} \frac{\partial \mathbf{q}}{\partial \mathbf{r}}, \quad \mathbf{B} = \left(\frac{\partial \mathbf{q}}{\partial \mathbf{r}} \right)^{-1} \frac{\partial \mathbf{G}}{\partial \mathbf{q}} \frac{\partial \mathbf{q}}{\partial \mathbf{r}}, \quad \mathbf{C} = \left(\frac{\partial \mathbf{q}}{\partial \mathbf{r}} \right)^{-1} \frac{\partial \mathbf{H}}{\partial \mathbf{q}} \frac{\partial \mathbf{q}}{\partial \mathbf{r}}. \quad (13)$$

The matrix \mathbf{A} has the elements

$$\mathbf{A} = - \begin{pmatrix} U & \rho \xi_x & \rho \xi_y & \rho \xi_z & 0 \\ 0 & U & 0 & 0 & \xi_x / \rho \\ 0 & 0 & U & 0 & \xi_y / \rho \\ 0 & 0 & 0 & U & \xi_z / \rho \\ 0 & \rho a^2 \xi_x & \rho a^2 \xi_y & \rho a^2 \xi_z & U \end{pmatrix}. \quad (14)$$

\mathbf{B} is obtained by replacing U and ξ with V and η . \mathbf{C} is obtained by using W and ζ instead of U and ξ .

2.2.1 The channel in- and outlet

We first consider the boundary conditions for $\zeta = 0$ and $\zeta = 1$, the inflow and outflow boundaries. Furthermore, we assume that the flow field only depends on ζ , i.e.,

$$\frac{\partial \mathbf{r}}{\partial \tau} - \mathbf{C} \frac{\partial \mathbf{r}}{\partial \zeta} = 0. \quad (15)$$

Linearizing these equations around \mathbf{r}_0 , i. e., $\mathbf{r} = \mathbf{r}_0 + \mathbf{r}'$, yields

$$\frac{\partial \mathbf{r}'}{\partial \tau} - \mathbf{C} \frac{\partial \mathbf{r}'}{\partial \zeta} = 0, \quad (16)$$

where

$$\mathbf{C} = \mathbf{C}(\mathbf{r}_0)$$

$$\mathbf{r}' = \begin{pmatrix} \rho' \\ u' \\ v' \\ w' \\ p' \end{pmatrix}.$$

Note that \mathbf{r}_0 is assumed to be a *constant*, i.e., it does not depend on the space coordinates. Hence, \mathbf{C} is a constant matrix. Since the Euler equations are hyperbolic, the matrix \mathbf{C} can be diagonalized by a similarity transformation such that

$$\frac{\partial \hat{\mathbf{r}}'}{\partial \tau} + \mathbf{\Lambda} \frac{\partial \hat{\mathbf{r}}'}{\partial \zeta} = 0, \quad (17)$$

where

$$\mathbf{\Lambda} = -\mathbf{T}^{-1}\mathbf{C}\mathbf{T} = \begin{pmatrix} W_0 & 0 & 0 & 0 & 0 \\ 0 & W_0 & 0 & 0 & 0 \\ 0 & 0 & W_0 & 0 & 0 \\ 0 & 0 & 0 & W_0 + \tilde{a}_0 & 0 \\ 0 & 0 & 0 & 0 & W_0 - \tilde{a}_0 \end{pmatrix}. \quad (18)$$

The variable W_0 is the previously defined contravariant velocity, and $\tilde{a}_0 = a_0|\nabla\zeta|_2$, a_0 being the speed of sound. The variable vector $\hat{\mathbf{r}}' = \mathbf{T}^{-1}\mathbf{r}'$ is referred to as the *characteristic* variable vector. Let

$$\begin{cases} \tilde{\zeta}_x = \zeta_x/|\nabla\zeta|_2 \\ \tilde{\zeta}_y = \zeta_y/|\nabla\zeta|_2 \\ \tilde{\zeta}_z = \zeta_z/|\nabla\zeta|_2 \end{cases}.$$

By a different scaling of the similarity transformation in [9]

$$\mathbf{T} = \begin{pmatrix} -\tilde{\zeta}_y & \tilde{\zeta}_x & \tilde{\zeta}_z/a_0^2 & 1/(2a_0^2) & 1/(2a_0^2) \\ \tilde{\zeta}_z & 0 & \tilde{\zeta}_y/a_0^2 & \tilde{\zeta}_x/(2\rho_0 a_0) & -\tilde{\zeta}_x/(2\rho_0 a_0) \\ 0 & \tilde{\zeta}_z & -\tilde{\zeta}_x/a_0^2 & \tilde{\zeta}_y/(2\rho_0 a_0) & -\tilde{\zeta}_y/(2\rho_0 a_0) \\ -\tilde{\zeta}_x & -\tilde{\zeta}_y & 0 & \tilde{\zeta}_z/(2\rho_0 a_0) & -\tilde{\zeta}_z/(2\rho_0 a_0) \\ 0 & 0 & 0 & 1/2 & 1/2 \end{pmatrix} \quad (19)$$

and

$$\mathbf{T}^{-1} = \begin{pmatrix} -\tilde{\zeta}_y & \tilde{\zeta}_z & 0 & -\tilde{\zeta}_x & \tilde{\zeta}_y/a_0^2 \\ \tilde{\zeta}_x & 0 & \tilde{\zeta}_z & -\tilde{\zeta}_y & -\tilde{\zeta}_x/a_0^2 \\ a_0^2\tilde{\zeta}_z & a_0^2\tilde{\zeta}_y & -a_0^2\tilde{\zeta}_x & 0 & -\tilde{\zeta}_z \\ 0 & \rho_0 a_0\tilde{\zeta}_x & \rho_0 a_0\tilde{\zeta}_y & \rho_0 a_0\tilde{\zeta}_z & 1 \\ 0 & -\rho_0 a_0\tilde{\zeta}_x & -\rho_0 a_0\tilde{\zeta}_y & -\rho_0 a_0\tilde{\zeta}_z & 1 \end{pmatrix}. \quad (20)$$

Hence,

$$\hat{\mathbf{r}}' = \begin{pmatrix} \phi_1 \\ \phi_2 \\ \phi_3 \\ \phi_4 \\ \phi_5 \end{pmatrix} = \begin{pmatrix} -\rho'\tilde{\zeta}_y + u'\tilde{\zeta}_z - w'\tilde{\zeta}_x + p'\tilde{\zeta}_y/a_0^2 \\ \rho'\tilde{\zeta}_x + v'\tilde{\zeta}_z - w'\tilde{\zeta}_y - p'\tilde{\zeta}_x/a_0^2 \\ \rho'a_0^2\tilde{\zeta}_z + u'a_0^2\tilde{\zeta}_y - v'a_0^2\tilde{\zeta}_x - p'\tilde{\zeta}_z \\ u'\rho_0 a_0\tilde{\zeta}_x + v'\rho_0 a_0\tilde{\zeta}_y + w'\rho_0 a_0\tilde{\zeta}_z + p' \\ -u'\rho_0 a_0\tilde{\zeta}_x - v'\rho_0 a_0\tilde{\zeta}_y - w'\rho_0 a_0\tilde{\zeta}_z + p' \end{pmatrix}. \quad (21)$$

Thus, the problem of solving the linearized problem (16) implies solving the scalar model equation

$$\frac{\partial\phi}{\partial\tau} + \nu\frac{\partial\phi}{\partial\zeta} = 0, \quad (22)$$

where ν is an eigenvalue of $\mathbf{\Lambda}$. The solution of the quarter plane problem

$$\begin{cases} \frac{\partial\phi}{\partial\tau} + \nu\frac{\partial\phi}{\partial\zeta} = 0, & \tau > 0, \quad \zeta > 0 \\ \phi = f(\zeta), & \tau = 0 \\ \phi = g(\tau), & \zeta = 0 \end{cases} \quad (23)$$

must be constant along the characteristic lines

$$\zeta - \nu\tau = M, \quad (24)$$

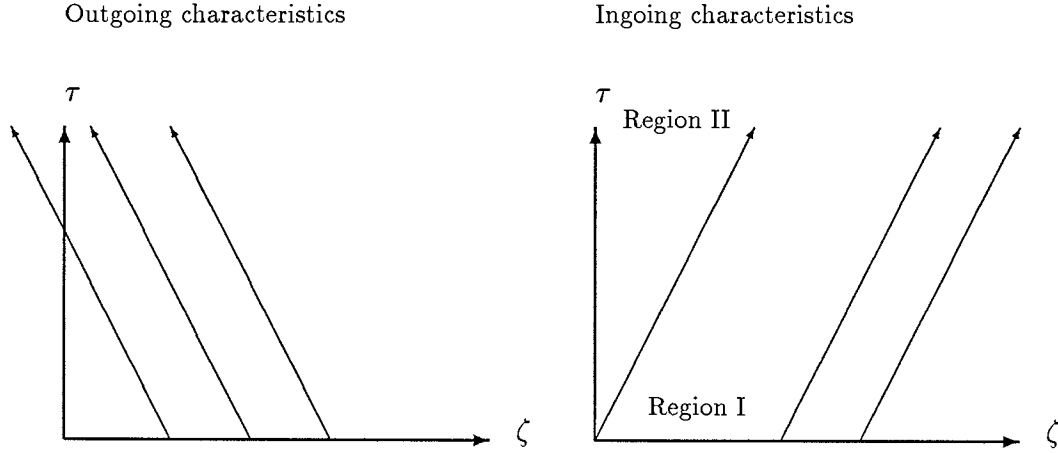


Figure 1: Domain of Influence of Characteristics with Negative and Positive Slopes

where M is a parameter and the coefficient ν is a constant. Solving for τ yields

$$\tau = \frac{1}{\nu}\zeta - \frac{M}{\nu}. \quad (25)$$

The situation depends critically on the sign of the eigenvalue ν . If ν is non-positive the solution will be completely determined by the initial conditions given along the positive ζ -axis. No boundary conditions are needed at $\zeta = 0$. In fact, no boundary condition could be prescribed unless it is compatible with the initial data. However, when the sign of ν is positive the quarter plane will be divided into two regions: one in which the solution depends on the initial data, and one in which the solution is determined by the boundary conditions at $\zeta = 0$, see Figure 1. The eigenvalue ν takes the following values:

$$\begin{aligned} \nu_1 &= W \\ \nu_2 &= W \\ \nu_3 &= W \\ \nu_4 &= W + \tilde{a} \\ \nu_5 &= W - \tilde{a}. \end{aligned}$$

The necessity of inflow boundary conditions depends on data through the contravariant velocity W . The outflow boundary conditions are treated analogously. *One* way of having a well posed problem is to prescribe only those variables corresponding to *ingoing* characteristics:

- (i) Subsonic inflow: $0 < W \leq \tilde{a} \Rightarrow \nu_j > 0, j = 1, \dots, 4, \nu_5 \leq 0$.
Prescribe the characteristic variables ϕ_1, ϕ_2, ϕ_3 and ϕ_4 .

- (ii) Subsonic outflow: $0 \leq W < \tilde{a} \Rightarrow \nu_1 \geq 0, \nu_2 \geq 0, \nu_3 \geq 0, \nu_4 > 0, \nu_5 < 0$.
Prescribe the scalar characteristic variable ϕ_5 .
- (iii) Supersonic inflow: $0 < \tilde{a} < W \Rightarrow \nu_j > 0, j = 1, \dots, 5$.
Prescribe all characteristic variables, i. e., prescribe all original variables.
- (iv) Supersonic outflow: $0 < \tilde{a} \leq W \Rightarrow \nu_j > 0, j = 1, \dots, 4, \nu_5 \geq 0$.
Prescribe no characteristic variables, i. e., prescribe no original variables.

2.2.2 The channel walls

The particle trajectories in four dimensions are defined by $(t, x(t), y(t), z(t))$, and the velocity field is $(1, u, v, w)$. The geometry is such that the solid walls of the channel are described by the level curves $\xi(t, x, y, z) = \text{const}$ and $\eta(t, x, y, z) = \text{const}$ with normal directions $\nabla'\xi$ and $\nabla'\eta$, respectively. ∇' is the four-dimensional gradient operator

$$\nabla'^T = \left(\frac{\partial}{\partial t} \quad \frac{\partial}{\partial x} \quad \frac{\partial}{\partial y} \quad \frac{\partial}{\partial z} \right). \quad (26)$$

The scalar product of the four-dimensional velocity field and the normal vector $\nabla'\xi$ is the contravariant velocity U , equation (9). Consequently, $U = 0$ at the boundaries described by $\xi(t, x, y, z) = 0$ and $\xi(t, x, y, z) = 1$. Similarly, $V = 0$ at the boundaries $\eta(t, x, y, z) = 0$ and $\eta(t, x, y, z) = 1$. At each solid boundary *one* boundary condition is prescribed.

We now show by using the energy method, that these boundary conditions lead to a well posed problem. Consider equation (12) in one dimension. This equation is obtained formally by setting $\mathbf{C} = \mathbf{B} = \mathbf{0}$. We only consider the linear problem and treat the entries of \mathbf{A} as constants. There exists a constant matrix \mathbf{S} [9] such that $\mathbf{S}^{-1}\mathbf{A}\mathbf{S}$ is symmetric. In the ξ -direction the equation is

$$\frac{\partial}{\partial \tau} \mathbf{S}^{-1} \mathbf{r}' = \mathbf{S}^{-1} \mathbf{A} \mathbf{S} \frac{\partial}{\partial \xi} \mathbf{S}^{-1} \mathbf{r}'. \quad (27)$$

We choose the symmetrizer as

$$\mathbf{S} = \begin{pmatrix} \rho_0 & \rho_0 & 0 & 0 & \rho_0 \\ 0 & a_0 & 0 & 0 & -a_0 \\ 0 & 0 & \sqrt{2}a_0 & 0 & 0 \\ 0 & 0 & 0 & \sqrt{2}a_0 & 0 \\ 0 & \rho_0 a_0^2 & 0 & 0 & \rho_0 a_0^2 \end{pmatrix} \quad (28)$$

with the inverse

$$\mathbf{S}^{-1} = \begin{pmatrix} 1/\rho_0 & 0 & 0 & 0 & -1/(\rho_0 a_0^2) \\ 0 & 1/(2a_0) & 0 & 0 & 1/(2\rho_0 a_0^2) \\ 0 & 0 & 1/(\sqrt{2}a_0) & 0 & 0 \\ 0 & 0 & 0 & 1/(\sqrt{2}a_0) & 0 \\ 0 & -1/(2a_0) & 0 & 0 & 1/(2\rho_0 a_0^2) \end{pmatrix}. \quad (29)$$

A solution of the symmetrized problem exists if and only if there is a solution to the non-symmetrized problem. Let $\tilde{\mathbf{r}}' = \mathbf{S}^{-1}\mathbf{r}'$. Then

$$\frac{\partial}{\partial \tau} \|\tilde{\mathbf{r}}'\|_2^2 = 2(\tilde{\mathbf{r}}', \tilde{\mathbf{r}}'_\tau) = 2(\tilde{\mathbf{r}}', \mathbf{S}^{-1}\mathbf{A}\mathbf{S}\tilde{\mathbf{r}}'_\xi). \quad (30)$$

Integrating this expression by parts leaves only the boundary terms, since $\mathbf{S}^{-1}\mathbf{A}\mathbf{S}$ is symmetric.

$$\frac{\partial}{\partial \tau} \|\tilde{\mathbf{r}}'\|_2^2 = 2(\tilde{\mathbf{r}}', \mathbf{S}^{-1}\mathbf{A}\mathbf{S}\tilde{\mathbf{r}}'_\xi) = \left[\tilde{\mathbf{r}}'^T \mathbf{S}^{-1}\mathbf{A}\mathbf{S}\tilde{\mathbf{r}}' \right]_{\xi=0}^{\xi=1}. \quad (31)$$

From the definitions of \mathbf{A} and \mathbf{r}' together with equations (28) and (29) and $\xi \in [0, 1]$, it follows that

$$\begin{aligned} \tilde{\mathbf{r}}'^T \mathbf{S}^{-1}\mathbf{A}\mathbf{S}\tilde{\mathbf{r}}' = & -U_0 \left\{ \frac{\rho'^2}{\rho_0^2} - \frac{2\rho'p'}{\rho_0^2 a_0^2} + \frac{3p'^2}{2\rho_0^2 a_0^4} + \frac{1}{2a_0^2} (u'^2 + v'^2 + w'^2) \right\} \\ & -U' \left\{ \frac{p'}{\rho_0 a_0^2} \right\} \end{aligned} \quad (32)$$

or

$$\tilde{\mathbf{r}}'^T \mathbf{S}^{-1}\mathbf{A}\mathbf{S}\tilde{\mathbf{r}}' = -U_0 h_0(\xi, \tau) - U' h_1(\xi, \tau), \quad (33)$$

since ρ', u', v', w' and p' all are functions of ξ and τ . U_0 is the reference level around which we have linearized the problem. At a solid boundary it is natural to choose $U_0 = 0$. This choice holds *even* if the boundary is not constant in time since

$$U_0 = \xi_t + u_0 \xi_x + v_0 \xi_y + w_0 \xi_z.$$

The variable ξ_t describes how the geometry moves with time. Note that

$$U' = u' \xi_x + v' \xi_y + w' \xi_z.$$

Thus, U' does not depend on ξ_t . This is an immediate consequence of the fact that the first component of the four-dimensional velocity field is a constant, namely 1. Hence

$$\left[\tilde{\mathbf{r}}'^T \mathbf{S}^{-1}\mathbf{A}\mathbf{S}\tilde{\mathbf{r}}' \right]_{\xi=0}^{\xi=1} = -U'(1, \tau) h_1(1, \tau) + U'(0, \tau) h_1(0, \tau). \quad (34)$$

From the above expression and equation (31), setting $U' = 0$ at the boundaries implies $\|\tilde{\mathbf{r}}'(\tau)\|_2 = \|\tilde{\mathbf{r}}'(0)\|_2$ for $\tau > 0$, which gives $\|\mathbf{r}'(\tau)\|_2 \leq \text{const}$, since \mathbf{S}^{-1} is a bounded operator. The problem is well posed.

2.3 Symmetry Properties

We assume a time independent geometry. Since the channel is a twisted parallelepiped, it is natural to assume that the solution possesses some kind of symmetry properties. The coordinate transformation

$$\begin{cases} x(\xi, \eta, \zeta) &= \xi \cos(\omega\zeta) - \eta \sin(\omega\zeta) \\ y(\xi, \eta, \zeta) &= \xi \sin(\omega\zeta) + \eta \cos(\omega\zeta) \\ z(\xi, \eta, \zeta) &= \zeta \end{cases} \quad (35)$$

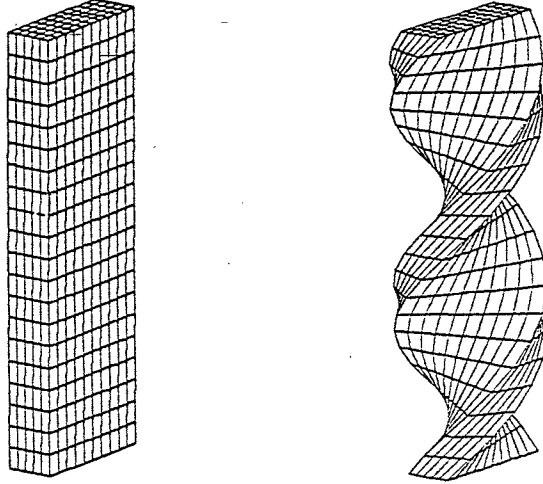


Figure 2: Computational and Physical Domain

describes a twisted parallelepiped a twisting factor of ω . Using equation (35) it is readily established that

$$\begin{cases} \xi_t = 0 \\ \xi_x = \cos(\omega\zeta) \\ \xi_y = \sin(\omega\zeta) \\ \xi_z = \omega\eta \end{cases} \begin{cases} \eta_t = 0 \\ \eta_x = -\sin(\omega\zeta) \\ \eta_y = \cos(\omega\zeta) \\ \eta_z = -\omega\xi \end{cases} \begin{cases} \zeta_t = 0 \\ \zeta_x = 0 \\ \zeta_y = 0 \\ \zeta_z = 1. \end{cases} \quad (36)$$

This gives the flux vectors

$$\mathbf{F} = - \begin{pmatrix} \rho U \\ \rho u U + p \cos(\omega\zeta) \\ \rho v U + p \sin(\omega\zeta) \\ \rho w U + p\omega\eta \\ (e + p)U \end{pmatrix} \quad (37)$$

$$\mathbf{G} = - \begin{pmatrix} \rho V \\ \rho u V - p \sin(\omega\zeta) \\ \rho v V + p \cos(\omega\zeta) \\ \rho w V - p\omega\xi \\ (e + p)V \end{pmatrix} \quad (38)$$

$$\mathbf{H} = - \begin{pmatrix} \rho W \\ \rho u W \\ \rho v W \\ \rho w W + p \\ (e + p)W \end{pmatrix}. \quad (39)$$

Replacing ξ and η by $-\xi$ and $-\eta$ in equation (1) yields

$$\frac{\partial \mathbf{q}}{\partial \tau} = -\frac{\partial \mathbf{F}}{\partial \xi} - \frac{\partial \mathbf{G}}{\partial \eta} + \frac{\partial \mathbf{H}}{\partial \zeta}, \quad (40)$$

where the flux vectors are defined by (37), (38) and (39). All variables are evaluated at the point $(-\xi, -\eta, \zeta)$. Define

$$\begin{cases} \bar{u}(\xi, \eta, \zeta) = -u(-\xi, -\eta, \zeta) \\ \bar{v}(\xi, \eta, \zeta) = -v(-\xi, -\eta, \zeta) \\ \bar{w}(\xi, \eta, \zeta) = w(-\xi, -\eta, \zeta) \end{cases} . \quad (41)$$

Using this definition and equations (9) and (36) it follows that

$$\begin{cases} U(-\xi, -\eta, \zeta) = -\bar{u} \cos(\omega \zeta) - \bar{v} \sin(\omega \zeta) - \bar{w} \omega \eta = -\bar{U} \\ V(-\xi, -\eta, \zeta) = \bar{u} \sin(\omega \zeta) - \bar{v} \cos(\omega \zeta) + \bar{w} \omega \xi = -\bar{V} \\ W(-\xi, -\eta, \zeta) = \bar{w} = \bar{W} \end{cases} . \quad (42)$$

Finally, we define

$$\begin{cases} \bar{\rho}(\xi, \eta, \zeta) = \rho(-\xi, -\eta, \zeta) \\ \bar{p}(\xi, \eta, \zeta) = p(-\xi, -\eta, \zeta) \\ \bar{e}(\xi, \eta, \zeta) = e(-\xi, -\eta, \zeta) \end{cases} . \quad (43)$$

Using definitions (41), (43) and equation (42) in equation (40) yields the original Euler equations, in which each variable has been replaced by its barred counterpart. At the inflow boundary $u = v = 0$, which, according to equation (41), is equivalent to prescribing $\bar{u} = \bar{v} = 0$. For the remaining three variables combinations of ρ, w and p are prescribed as needed. It is clear that equation (15) holds for the barred quantities as well. The inflow boundary conditions remain unchanged. At the outflow at most one boundary condition is needed (one combination of ρ, w and p). Thus, the outflow boundary conditions are valid for the barred variables. According to equation (42) \bar{U} and \bar{V} are zero at the solid walls, if and only if U and V are zero at the wall boundaries. The boundary conditions remain unchanged, and (2) is a solution of (1), if and only if

$$\bar{\mathbf{q}} = |\mathbf{J}|^{-1} \begin{pmatrix} \bar{\rho} \\ \bar{\rho} \bar{u} \\ \bar{\rho} \bar{v} \\ \bar{\rho} \bar{w} \\ \bar{e} \end{pmatrix} \quad (44)$$

also satisfies (1). A necessary condition for uniqueness is that the solution of (1) satisfies the symmetry conditions

$$\begin{cases} \rho(\xi, \eta, \zeta) = \rho(-\xi, -\eta, \zeta) \\ u(\xi, \eta, \zeta) = -u(-\xi, -\eta, \zeta) \\ v(\xi, \eta, \zeta) = -v(-\xi, -\eta, \zeta) \\ w(\xi, \eta, \zeta) = w(-\xi, -\eta, \zeta) \\ e(\xi, \eta, \zeta) = e(-\xi, -\eta, \zeta) \end{cases} . \quad (45)$$

The following proposition has been proved:

Proposition 2.1 *Suppose data satisfies (45). Then, if there is a solution to (1) for which the symmetry condition (45) does not hold, this solution cannot be unique.*

3 Artificial viscosity

We have chosen a finite difference method with explicit time-stepping. Centered spatial difference operators are used in the interior and one-sided operators at the boundaries. Non-linear phenomena, such as shocks and aliasing, cause numerical instabilities. To remedy this situation numerical dissipation is introduced. It is created through a fourth-order difference term (in \mathbf{q}), which is turned off near shocks so as not to cause any spurious effects. At shocks we use a second-order difference to filter the solution. In this section we consider three different dissipation operators at and near the boundary: a positive definite operator [8], a semidefinite operator [4], and an indefinite operator. The operators only differ in the treatment of the boundary, and can be represented by matrices of a bandwidth determined by the difference operator in the interior of the domain. We consider three different factorizations of the semidefinite operator, in addition to the unfactored operator. The different factorizations yield dissipation operators with different stability properties.

3.1 Interior Points

The semidiscrete Euler equations for a time independent geometry, including artificial viscosity, are

$$\frac{\partial \check{\mathbf{q}}_{jkl}}{\partial \tau} = |\mathbf{J}_{jkl}| [D_0^\xi \mathbf{F}_{jkl} + D_0^\eta \mathbf{G}_{jkl} + D_0^\zeta \mathbf{H}_{jkl} - D_{AV} \check{\mathbf{q}}_{jkl}], \quad (46)$$

where

$$\begin{cases} \mathbf{F}_{jkl} &= \mathbf{F}(\mathbf{q}_{jkl}) \\ \mathbf{G}_{jkl} &= \mathbf{G}(\mathbf{q}_{jkl}) \\ \mathbf{H}_{jkl} &= \mathbf{H}(\mathbf{q}_{jkl}) \end{cases} .$$

The discrete difference operators D_0^ξ , Δ_+^ξ and Δ_-^ξ are defined by

$$\begin{cases} D_0^\xi \phi_{jkl} &= (\phi_{j+1,kl} - \phi_{j-1,kl}) / (2\Delta\xi) \\ \Delta_+^\xi \phi_{jkl} &= \phi_{j+1,kl} - \phi_{jkl} \\ \Delta_-^\xi \phi_{jkl} &= \phi_{jkl} - \phi_{j-1,kl} \end{cases} . \quad (47)$$

The remaining operators are defined analogously. Furthermore, we assume a time independent geometry for which

$$\Delta\xi = \Delta\eta = \Delta\zeta = 1.$$

The complete coordinate transformation will be discussed in detail in section 3.3. The following formulations of $D_{AV} \check{\mathbf{q}}_{jkl}$ have been proposed [5, 4, 8]:

$$D_{AV} \check{\mathbf{q}}_{jkl} = |\mathbf{J}_{jkl}|^{-1} \sigma_{jkl} \{ \varepsilon^\xi [\Delta_+^\xi \Delta_-^\xi]^2 + \varepsilon^\eta [\Delta_+^\eta \Delta_-^\eta]^2 + \varepsilon^\zeta [\Delta_+^\zeta \Delta_-^\zeta]^2 \} \check{\mathbf{q}}_{jkl} \quad (48)$$

$$\begin{aligned}
D_{AV} \check{q}_{jkl} &= \Delta_-^\xi [|\mathbf{J}_{jkl}|^{-1} \sigma_{jkl} \epsilon^\xi \Delta_+^\xi \Delta_-^\xi \Delta_+^\xi \check{q}_{jkl}] \\
&+ \Delta_-^\eta [|\mathbf{J}_{jkl}|^{-1} \sigma_{jkl} \epsilon^\eta \Delta_+^\eta \Delta_-^\eta \Delta_+^\eta \check{q}_{jkl}] \\
&+ \Delta_-^\zeta [|\mathbf{J}_{jkl}|^{-1} \sigma_{jkl} \epsilon^\zeta \Delta_+^\zeta \Delta_-^\zeta \Delta_+^\zeta \check{q}_{jkl}]
\end{aligned} \tag{49}$$

$$\begin{aligned}
D_{AV} \check{q}_{jkl} &= \Delta_-^\xi \Delta_+^\xi [|\mathbf{J}_{jkl}|^{-1} \sigma_{jkl} \epsilon^\xi \Delta_-^\xi \Delta_+^\xi \check{q}_{jkl}] \\
&+ \Delta_-^\eta \Delta_+^\eta [|\mathbf{J}_{jkl}|^{-1} \sigma_{jkl} \epsilon^\eta \Delta_-^\eta \Delta_+^\eta \check{q}_{jkl}] \\
&+ \Delta_-^\zeta \Delta_+^\zeta [|\mathbf{J}_{jkl}|^{-1} \sigma_{jkl} \epsilon^\zeta \Delta_-^\zeta \Delta_+^\zeta \check{q}_{jkl}],
\end{aligned} \tag{50}$$

where

$$\check{q}_{jkl} = |\mathbf{J}_{jkl}| \mathbf{q}_{jkl} \tag{51}$$

$$\sigma_{jkl} = |U_{jkl}| + |V_{jkl}| + |W_{jkl}| + a_{jkl} (|\nabla \xi_{jkl}|_2 + |\nabla \eta_{jkl}|_2 + |\nabla \zeta_{jkl}|_2) \tag{52}$$

$$\epsilon^\xi = \epsilon^\eta = \epsilon^\zeta = \vartheta_4 \tag{53}$$

with no smoothing at shocks. The constant ϑ_4 has a value of approximately 0.01. For a better treatment of shocks we add one of the following quantities to $D_{AV} \check{q}_{jkl}$:

$$-|\mathbf{J}_{jkl}|^{-1} \sigma_{jkl} \{ \epsilon_{jkl}^\xi \Delta_+^\xi \Delta_-^\xi + \epsilon_{jkl}^\eta \Delta_+^\eta \Delta_-^\eta + \epsilon_{jkl}^\zeta \Delta_+^\zeta \Delta_-^\zeta \} \check{q}_{jkl} \tag{54}$$

$$-\Delta_-^\xi [|\mathbf{J}_{jkl}|^{-1} \sigma_{jkl} \epsilon_{jkl}^\xi \Delta_+^\xi \check{q}_{jkl}] - \Delta_-^\eta [|\mathbf{J}_{jkl}|^{-1} \sigma_{jkl} \epsilon_{jkl}^\eta \Delta_+^\eta \check{q}_{jkl}] - \Delta_-^\zeta [|\mathbf{J}_{jkl}|^{-1} \sigma_{jkl} \epsilon_{jkl}^\zeta \Delta_+^\zeta \check{q}_{jkl}]. \tag{55}$$

The coefficient in front of the difference operator in the ξ -direction is given by

$$\epsilon_{jkl}^\xi = \vartheta_2 \max(\Upsilon_{j+l,kl}^\xi, \Upsilon_{jkl}^\xi, \Upsilon_{j-1,kl}^\xi) \tag{56}$$

with

$$\Upsilon_{jkl}^\xi = \frac{|p_{j+1,kl} - 2p_{jkl} + p_{j-1,kl}|}{|p_{j+1,kl} + 2p_{jkl} + p_{j-1,kl}|}. \tag{57}$$

A typical value of the constant ϑ_2 is 1/4. The other coefficients are defined analogously. The max-function is used to increase the second-order dissipation coefficients near the shock. The fourth-order coefficients

$$\epsilon^\xi, \quad \epsilon^\eta, \quad \epsilon^\zeta$$

can no longer be treated as constants. Instead we set

$$\begin{aligned}
\epsilon^\xi &= \epsilon_{jkl}^\xi = \max(0, \vartheta_4 - \epsilon_{jkl}^\xi) \\
\epsilon^\eta &= \epsilon_{jkl}^\eta = \max(0, \vartheta_4 - \epsilon_{jkl}^\eta) \\
\epsilon^\zeta &= \epsilon_{jkl}^\zeta = \max(0, \vartheta_4 - \epsilon_{jkl}^\zeta).
\end{aligned} \tag{58}$$

Near shocks the pressure gradients are very strong, causing the max-function to switch off the fourth-order dissipation.

3.2 Boundary Points

In this section we define and determine the conservation properties and null spaces of the dissipation operator proposed by Eriksson [4], a positive definite operator [8] and an unsymmetric operator. The only difference between the three dissipation operators is in the handling of the boundaries. Furthermore, we also derive three different factorizations of the operator due to Eriksson.

A simple - but by no means complete - analysis of the discrete fourth-order dissipation can be based on the equation

$$\frac{\partial \phi}{\partial \tau} = \mathbf{D}_4 \phi, \quad (59)$$

where \mathbf{D}_4 is the matrix representation of the dissipation operator. To see if \mathbf{D}_4 is moment preserving in time, we study the equation

$$\frac{\partial Q_p}{\partial \tau} = \sum_{j=0}^{j=N} j^p \frac{\partial \phi_j}{\partial \tau} = \sum_{j=0}^{j=N} j^p D_4 \phi_j, \quad (60)$$

where D_4 is a fourth-order *scalar* operator, and Q_p is the p -th order moment defined by [4]

$$Q_p = \sum_{j=0}^{j=N} j^p \phi_j, \quad p \geq 0. \quad (61)$$

We use the notation D_4 for fourth-order operators at interior points as well as boundary points. The last equality in equation (60) follows from (59). We will determine the null space of the dissipation operators, and whether or not the dissipation operators are definite.

3.2.1 A positive semidefinite fourth-order dissipation operator.

Denote by $[\Delta_+ \Delta_-]^2$ the fourth-order operator in any direction. Applying this operator to an interior point yields

$$D_4 \phi_j = [\Delta_+ \Delta_-]^2 \phi_j = \phi_{j-2} - 4\phi_{j-1} + 6\phi_j - 4\phi_{j+1} + \phi_{j+2}. \quad (62)$$

Eriksson [4] has shown that for periodic boundary conditions this operator is positive semidefinite, preserves zeroth, first, second and third order moments, i.e., that equation (60) vanishes identically for $p = 0, 1, 2, 3$, and that the null space consists of all polynomials of degree less or equal to three. With the boundary conditions we consider, the fourth-order dissipation operators cannot be used as presented in section 3.1. Eriksson has suggested a procedure for specifying the boundary operators such that the total operator (including the boundary modifications) inherits as many of the properties as possible of the operator in the interior with periodic boundary conditions.

Hence, this operator is positive semidefinite. It preserves the zeroth and first order moments, and its null space is all polynomials of degree less or equal to one. The analysis of $\mathbf{D}_1^- \Sigma \mathbf{D}_3^+$ and $\mathbf{D}_1^+ \Sigma \mathbf{D}_3^-$ is more involved and will not be carried out here. The operators have different stability properties. Consider

$$\begin{aligned}\phi^T \mathbf{D}_1^- \Sigma \mathbf{D}_3^+ \phi &= (\mathbf{D}_1^- \Sigma \mathbf{D}_1^+ \phi)^T \mathbf{D}_2 \phi \\ \phi^T \mathbf{D}_1^+ \Sigma \mathbf{D}_3^- \phi &= (\mathbf{D}_1^+ \Sigma \mathbf{D}_1^- \phi)^T \mathbf{D}_2 \phi,\end{aligned}$$

where

$$\mathbf{D}_1^- \Sigma \mathbf{D}_1^+ \phi \neq \mathbf{D}_1^+ \Sigma \mathbf{D}_1^- \phi$$

The first choice yields a stable scheme, whereas the second choice is unstable. The factorization in (76) is the preferred choice. Table 1 summarizes the properties of the dissipation operators.

Dissipation Operator	Definiteness	Preservation of Moments	Dimension of Null Space
\mathbf{D}_4	positive semidefinite	\leq first order	2
$\tilde{\mathbf{D}}_4$	positive definite	none	0
$\bar{\mathbf{D}}_4$	indefinite	zeroth order	3
$\mathbf{D}_1^- \Sigma \mathbf{D}_3^+$			2
$\mathbf{D}_1^+ \Sigma \mathbf{D}_3^-$			2
$\mathbf{D}_1^- \mathbf{D}_1^+ \Sigma \mathbf{D}_2$	positive semidefinite	\leq first order	2

Table 1: Properties of the Dissipation Operators

3.3 Spatial Discretization

We have chosen a transformation between the physical and computational grids such that $\Delta\xi = \Delta\eta = \Delta\zeta = 1$, the origin of the physical coordinates coincides with the center of the channel cross-section at the inflow boundary, and the range of the computational coordinates is $0 \leq \xi_j \leq N_\xi$, $0 \leq \eta_k \leq N_\eta$ and $0 \leq \zeta_l \leq N_\zeta$. Denote the cross-sectional physical side lengths by L_x and L_y , and the physical channel length by L_z . The complete transformation between the computational and the physical grids $(\xi, \eta, \zeta) \rightarrow (x, y, z)$ is

$$\begin{cases} x = \xi' \cos(\omega(\zeta)/N_\zeta) - \eta' \sin(\omega(\zeta)/N_\zeta) \\ y = \xi' \sin(\omega(\zeta)/N_\zeta) + \eta' \cos(\omega(\zeta)/N_\zeta) \\ z = \zeta L_z / N_\zeta \end{cases}, \quad (77)$$

where

$$\begin{cases} \xi' &= (2\xi/N_\xi - 1) L_x/2 \\ \eta' &= (2\eta/N_\eta - 1) L_y/2 \end{cases} \quad (78)$$

and

$$\omega(\zeta) = \begin{cases} 0 & \zeta \in [0, \zeta_0) \\ \bar{\omega}(3\zeta_1 - \zeta_0 - 2\zeta)(\zeta - \zeta_0)^2(\zeta_1 - \zeta_0)^{-3} & \zeta \in [\zeta_0, \zeta_1) \\ \bar{\omega} & \zeta \in [\zeta_1, N_\zeta] \end{cases} \quad (79)$$

$\omega(\zeta)$ is a C^1 -spline on the interval $[0, N_\zeta]$. Introducing this spline function enables a C^1 -grid transformation, which is such that the homogeneous inflow condition $u = 0$, $v = 0$, $w = w_0$, where u , v and w denote the Cartesian velocity components, yields continuous velocity gradients even at the inflow boundary. The function $\omega(\zeta)$ describes how the twisting factor (angular frequency) increases from 0 to $\bar{\omega}$ along the ζ -axis, which coincides with the physical z -axis. We use

$$\bar{\omega} = 2\pi/N_\zeta.$$

All the metric coefficients are derived from (77), (78), (79) and

$$\mathbf{J}'' = \begin{pmatrix} \xi_x & \xi_y & \xi_z \\ \eta_x & \eta_y & \eta_z \\ \zeta_x & \zeta_y & \zeta_z \end{pmatrix} = \begin{pmatrix} x_\xi & x_\eta & x_\zeta \\ y_\xi & y_\eta & y_\zeta \\ z_\xi & z_\eta & z_\zeta \end{pmatrix}^{-1}. \quad (80)$$

3.4 Fourier Analysis

The explicit method limits the maximum size of the time step. To determine the upper limit of the time step we analyze the linearized, one-dimensional, Euler equations. The same analysis can be performed in three dimensions. Consider a uniform 1D-grid $\{\xi_j\}$, $j = 0, \dots, N$, where each ξ_j belongs to the interval $[0, L)$. Every function defined on the above grid can be interpolated by a trigonometric polynomial [2]

$$f(\xi) = \sum_{n=-s}^{s+\theta} c_n \exp(n \frac{\xi}{L} 2\pi i),$$

where

$$\begin{cases} \theta = 0, s = N/2 & \text{if } N \text{ is even} \\ \theta = 1, s = (N-1)/2 & \text{if } N \text{ is odd} \end{cases}$$

and

$$c_n = (N+1)^{-1} \sum_{j=0}^N f(\xi_j) \exp(-n \frac{\xi_j}{L} 2\pi i),$$

where $\xi_j = Lj/(N+1)$, and N is even for simplicity. For a linear problem, it suffices to consider one Fourier mode at a time. Moreover, in our computational domain $\Delta\xi = 1$, which is formally obtained by setting $L = N+1$. It is sufficient to consider solutions of the form

$$\mathbf{q}(\xi, \tau) = \bar{\mathbf{q}}(\tau) e^{i\kappa\xi},$$

where the wave number κ is given by

$$\kappa = \frac{2\pi n}{N+1}, \quad n = -\frac{N}{2}, \dots, \frac{N}{2}.$$

Consequently, $\kappa \in (-\pi, \pi)$ ($\kappa \in (-\pi, \pi]$ if N is odd).

In three space dimensions the Fourier mode decomposition can also be obtained by considering plane waves

$$\mathbf{q}(\xi, \eta, \zeta, \tau) = \bar{\mathbf{q}}(\tau) \exp i(\kappa_1 \xi + \kappa_2 \eta + \kappa_3 \zeta).$$

Using this expression in the semidiscrete, linearized Euler equations yields

$$\frac{\partial \bar{\mathbf{q}}(\tau)}{\partial \tau} = i(\sin(\kappa_1) \bar{\mathbf{F}} + \sin(\kappa_2) \bar{\mathbf{G}} + \sin(\kappa_3) \bar{\mathbf{H}}) \bar{\mathbf{q}}(\tau). \quad (81)$$

which can be diagonalized as

$$\frac{\partial \phi(\tau)}{\partial \tau} + i\nu_j \phi(\tau) = 0, \quad (82)$$

where

$$\begin{aligned} \nu_j &= \sin(\kappa_1)U + \sin(\kappa_2)V + \sin(\kappa_3)W, \quad j = 1, 2, 3 \\ \nu_4 &= \sin(\kappa_1)U + \sin(\kappa_2)V + \sin(\kappa_3)W \\ &+ a[(\sin(\kappa_1)\xi_x + \sin(\kappa_2)\eta_x + \sin(\kappa_3)\zeta_x)^2 + \\ &(\sin(\kappa_1)\xi_y + \sin(\kappa_2)\eta_y + \sin(\kappa_3)\zeta_y)^2 + \\ &(\sin(\kappa_1)\xi_z + \sin(\kappa_2)\eta_z + \sin(\kappa_3)\zeta_z)^2]^{1/2} \\ \nu_5 &= \sin(\kappa_1)U + \sin(\kappa_2)V + \sin(\kappa_3)W \\ &- a[(\sin(\kappa_1)\xi_x + \sin(\kappa_2)\eta_x + \sin(\kappa_3)\zeta_x)^2 + \\ &(\sin(\kappa_1)\xi_y + \sin(\kappa_2)\eta_y + \sin(\kappa_3)\zeta_y)^2 + \\ &(\sin(\kappa_1)\xi_z + \sin(\kappa_2)\eta_z + \sin(\kappa_3)\zeta_z)^2]^{1/2}. \end{aligned} \quad (83)$$

The eigenvalues $\nu_j, j = 1, 2, 3, 4, 5$ are constant, since $\bar{\mathbf{F}}, \bar{\mathbf{G}}$ and $\bar{\mathbf{H}}$ are *constant* operators in space and time.

3.5 Time Discretization

A three stage Runge-Kutta method is used to integrate the semidiscrete Euler equations in time. It belongs to a class of integration methods that can be written

$$\begin{cases} \check{\mathbf{q}}_{jkl}^0 &= \check{\mathbf{q}}_{jkl}^n \\ \check{\mathbf{q}}_{jkl}^1 &= \check{\mathbf{q}}_{jkl}^0 + \alpha_1 \Delta \tau \mathbf{R}(\check{\mathbf{q}}_{jkl}^0) \\ &\vdots \\ \check{\mathbf{q}}_{jkl}^m &= \check{\mathbf{q}}_{jkl}^0 + \alpha_m \Delta \tau \mathbf{R}(\check{\mathbf{q}}_{jkl}^{m-1}) \\ \check{\mathbf{q}}_{jkl}^{n+1} &= \check{\mathbf{q}}_{jkl}^m \end{cases}. \quad (84)$$

The vector \mathbf{R} is the right member of equation (46). For a three stage Runge-Kutta method $m = 3$. The steady solution is independent of the coefficients α_j and $\Delta \tau$. This property

also holds if $\Delta\tau$ is replaced by a local time step $\Delta\tau_{jkl}^n$. The coefficients α_j can be looked upon as acceleration parameters [3]. We have used $\alpha_1 = \alpha_2 = \alpha_3 = 1$. Applying this Runge-Kutta scheme to (82) yields

$$\phi^{n+1} = G(\nu_j \Delta\tau) \phi^n,$$

where

$$G(\nu_j \Delta\tau) = 1 - (\nu_j \Delta\tau)^2 - i(\nu_j \Delta\tau - (\nu_j \Delta\tau)^3).$$

It suffices to consider only the diagonalized equation (82), since the Runge-Kutta scheme results in a matrix polynomial of the right hand side of (81). It is irrelevant if we diagonalize (81) before applying the Runge-Kutta scheme, or after applying it. The stability criteria $|G(\nu_j \Delta\tau)| \leq 1, j = 1, 2, 3, 4, 5$ is equivalent to

$$|\nu_j| \Delta\tau \leq \sqrt{\frac{1}{2}(1 + \sqrt{5})} \equiv CFL, \quad (85)$$

where CFL is the Courant-Friedrichs-Lewy number. From the Cauchy-Schwartz inequality

$$|\nu_j| \leq |U| + |V| + |W| + a(|\nabla\xi|_2 + |\nabla\eta|_2 + |\nabla\zeta|_2), \quad j = 1, 2, 3, 4, 5,$$

and (85) will hold if

$$\Delta\tau \leq \frac{CFL}{|U| + |V| + |W| + a(|\nabla\xi|_2 + |\nabla\eta|_2 + |\nabla\zeta|_2)} \equiv \frac{CFL}{\sigma}, \quad (86)$$

where the definition of σ in (86) is the same as in (52). For the real problem σ varies in space, but (86) provides a condition for the local time step at each point. Most stability theorems assume *uniform* time steps, but interpreting the theorems locally often works well in practice. Note however that local time steps are *not* acceptable for time-dependent problems.

The linear analysis above is not sufficient. Stability cannot be obtained without artificial viscosity. The effect of the fourth-order artificial viscosity is to slightly shift the spectrum of the discrete space operator into the left half of the complex plane. Lowering the CFL -number slightly guarantees that $|G(\nu\Delta\tau)|$ is strictly less than one. From Figure 3 it is evident that the shifted spectrum will remain in the stability region of the three stage Runge-Kutta method, if the viscosity coefficient is sufficiently small.

3.6 Numerical Methods, Summary

In summary, the Euler flow equations are based on the twisted grid as defined by equations (77), (78) and (79), and the semidiscrete equations

$$\begin{aligned} \frac{\partial \check{q}_{jkl}}{\partial \tau} &= |\mathbf{J}_{jkl}| [D_0^\xi \mathbf{F}_{jkl} + D_0^\eta \mathbf{G}_{jkl} + D_0^\zeta \mathbf{H}_{jkl}] \\ &- \sigma_{jkl} \{ \epsilon_{jkl}^\xi [\Delta_+^\xi \Delta_-^\xi]^2 + \epsilon_{jkl}^\eta [\Delta_+^\eta \Delta_-^\eta]^2 + \epsilon_{jkl}^\zeta [\Delta_+^\zeta \Delta_-^\zeta]^2 \} \check{q}_{jkl} \\ &+ \sigma_{jkl} \{ \epsilon_{jkl}^\xi \Delta_+^\xi \Delta_-^\xi + \epsilon_{jkl}^\eta \Delta_+^\eta \Delta_-^\eta + \epsilon_{jkl}^\zeta \Delta_+^\zeta \Delta_-^\zeta \} \check{q}_{jkl} \end{aligned} \quad (87)$$

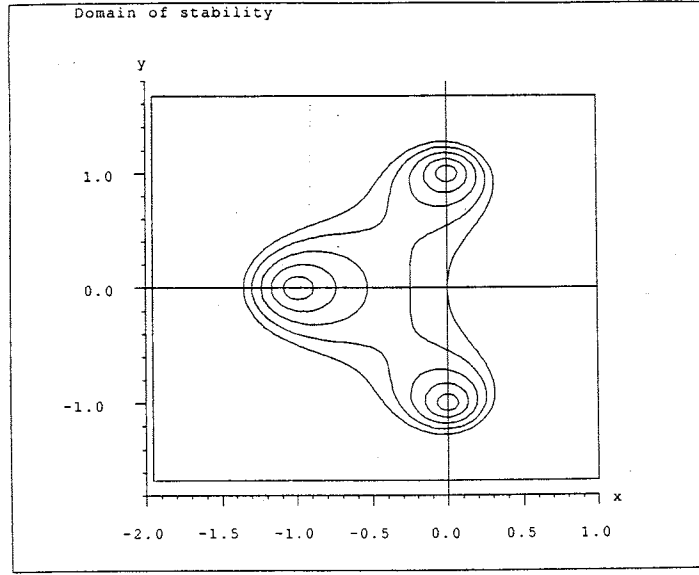


Figure 3: Stability Region of the Three Stage Runge Kutta Method

in non-conservative form and

$$\begin{aligned}
\frac{\partial \check{\mathbf{q}}_{jkl}}{\partial \tau} &= |\mathbf{J}_{jkl}| \{ D_0^\xi \mathbf{F}_{jkl} + D_0^\eta \mathbf{G}_{jkl} + D_0^\zeta \mathbf{H}_{jkl} \\
&- \Delta_-^\xi [|\mathbf{J}_{jkl}|^{-1} \sigma_{jkl} \epsilon_{jkl}^\xi \Delta_+^\xi \Delta_-^\xi \check{\mathbf{q}}_{jkl}] \\
&- \Delta_-^\eta [|\mathbf{J}_{jkl}|^{-1} \sigma_{jkl} \epsilon_{jkl}^\eta \Delta_+^\eta \Delta_-^\eta \check{\mathbf{q}}_{jkl}] \\
&- \Delta_-^\zeta [|\mathbf{J}_{jkl}|^{-1} \sigma_{jkl} \epsilon_{jkl}^\zeta \Delta_+^\zeta \Delta_-^\zeta \check{\mathbf{q}}_{jkl}] \\
&+ \Delta_-^\xi [|\mathbf{J}_{jkl}|^{-1} \sigma_{jkl} \epsilon_{jkl}^\xi \Delta_+^\xi \check{\mathbf{q}}_{jkl}] \\
&+ \Delta_-^\eta [|\mathbf{J}_{jkl}|^{-1} \sigma_{jkl} \epsilon_{jkl}^\eta \Delta_+^\eta \check{\mathbf{q}}_{jkl}] \\
&+ \Delta_-^\zeta [|\mathbf{J}_{jkl}|^{-1} \sigma_{jkl} \epsilon_{jkl}^\zeta \Delta_+^\zeta \check{\mathbf{q}}_{jkl}] \}
\end{aligned} \tag{88}$$

or

$$\begin{aligned}
\frac{\partial \check{\mathbf{q}}_{jkl}}{\partial \tau} &= |\mathbf{J}_{jkl}| \{ D_0^\xi \mathbf{F}_{jkl} + D_0^\eta \mathbf{G}_{jkl} + D_0^\zeta \mathbf{H}_{jkl} \\
&- \Delta_-^\xi \Delta_+^\xi [|\mathbf{J}_{jkl}|^{-1} \sigma_{jkl} \epsilon_{jkl}^\xi \Delta_-^\xi \Delta_+^\xi \check{\mathbf{q}}_{jkl}] \\
&- \Delta_-^\eta \Delta_+^\eta [|\mathbf{J}_{jkl}|^{-1} \sigma_{jkl} \epsilon_{jkl}^\eta \Delta_-^\eta \Delta_+^\eta \check{\mathbf{q}}_{jkl}] \\
&- \Delta_-^\zeta \Delta_+^\zeta [|\mathbf{J}_{jkl}|^{-1} \sigma_{jkl} \epsilon_{jkl}^\zeta \Delta_-^\zeta \Delta_+^\zeta \check{\mathbf{q}}_{jkl}] \\
&+ \Delta_-^\xi [|\mathbf{J}_{jkl}|^{-1} \sigma_{jkl} \epsilon_{jkl}^\xi \Delta_+^\xi \check{\mathbf{q}}_{jkl}] \\
&+ \Delta_-^\eta [|\mathbf{J}_{jkl}|^{-1} \sigma_{jkl} \epsilon_{jkl}^\eta \Delta_+^\eta \check{\mathbf{q}}_{jkl}] \\
&+ \Delta_-^\zeta [|\mathbf{J}_{jkl}|^{-1} \sigma_{jkl} \epsilon_{jkl}^\zeta \Delta_+^\zeta \check{\mathbf{q}}_{jkl}] \}
\end{aligned} \tag{89}$$

in conservative form. Equation (89) has not yet been implemented. The reciprocal cell volume at point jkl is computed from equation (3), \mathbf{F}_{jkl} , \mathbf{G}_{jkl} and \mathbf{H}_{jkl} are given by equations (6), (7) and (8). The vector $\check{\mathbf{q}}_{jkl}$ is given by equation (51), σ_{jkl} by equation (52), ϵ_{jkl} by equation (58), ϵ_{jkl} by equation (56), and the difference operators for interior and boundary points are given by equation (47). For boundary points higher order difference

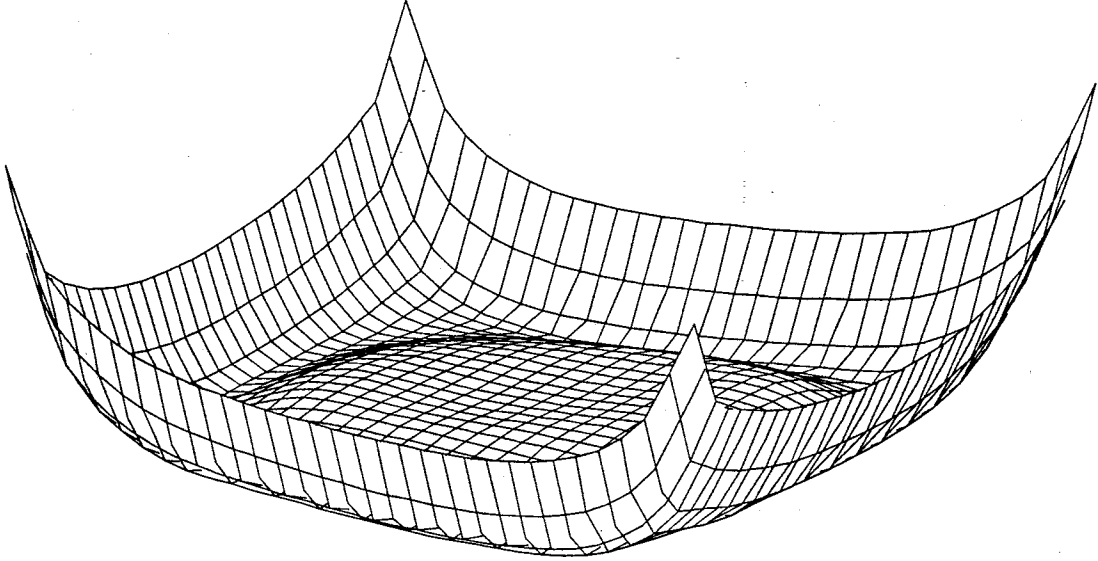


Figure 4: Entropy Distribution at Outflow Boundary, Operator \tilde{D}_4

operators are modified as defined by one of equations (65), (66) or (67) and by (75). For the conservative form the fourth-order operator is modified according to equations (68) and (69). The in- and outflow boundary conditions are defined by equation (21) and by the discussion in section 2.2. At the solid boundaries the normal component of the velocity field is zero.

4 Simulation results

The effects on the entropy distribution, the flow, and the convergence rate of the different dissipation operators for the Euler equations were studied for a twisted channel of rectangular cross-section. The channel dimensions were $0.035 \times 0.0175 \times 0.140 \text{ m}^3$. The grid sizes ranged from $32 \times 32 \times 32$ to $32 \times 32 \times 64$, with the total number of grid points ranging from 32,768 to 65,536 points. The demonstrated performance for a fully configured Connection Machine system model CM-2 is 1.1 Gflops/s in single-precision.

Since no shocks are present, the flow must be isentropic throughout the channel, provided that inflow data is isentropic. We compute the entropy as

$$S = c_v \log \left[\frac{p}{(\gamma - 1)\rho^\gamma} \right], \quad (90)$$

which is valid for a polytropic gas [1]. Prescribing constant pressure and density at the inflow boundary ensures that the inflow data is isentropic.

Figure 4 and Table 2 show how the entropy piles up at the solid walls for the operator

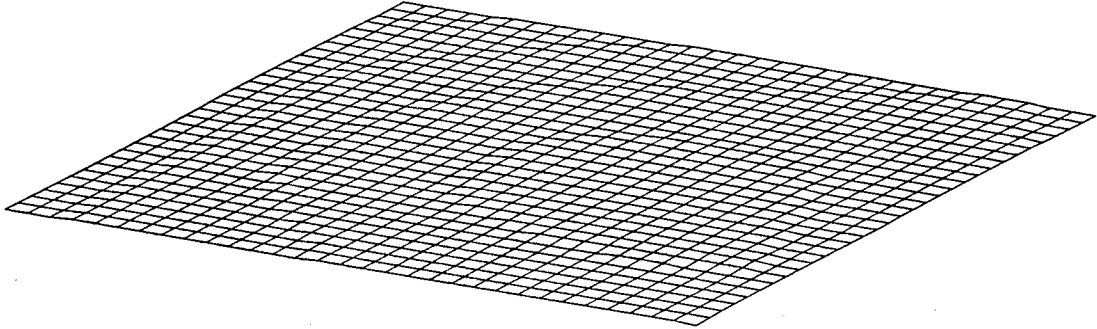


Figure 5: Entropy Distribution at Outflow Boundary, Operator $\mathbf{D}_1^- \Sigma \mathbf{D}_3^+$

$\tilde{\mathbf{D}}_4$. The entropy distribution for the operator $\mathbf{D}_1^- \Sigma \mathbf{D}_3^+$ is shown in Figure 5. The scale is the same in both figures. Table 2 also shows that $\tilde{\mathbf{D}}_4$ and \mathbf{D}_4 are entropy preserving.

An indication of the sensitivity of the dissipation operators to perturbations in the inflow data can be obtained from observations of w at the outflow. We studied two cases: completely irrotational inflow, and an inflow with a slight rotation. For the irrotational flow the normalized inflow data is $u = 0$, $v = 0$ and $w = 1$. In the second test case $u \neq 0$ and $v \neq 0$, but small, at the solid walls of the inlet. All interior points at the inflow boundary are the same as for the irrotational case. From the contour plots it is apparent that the choice of dissipation operator *does* affect the flow, even if the operator is entropy preserving. Comparing the perturbed and the non-perturbed flows, we note that the conservative operator $\mathbf{D}_1^- \Sigma \mathbf{D}_3^+$ appears to be more stable than the non-conservative operators \mathbf{D}_4 and $\tilde{\mathbf{D}}_4$. In fact, Figures 8 and 11 indicate that $\tilde{\mathbf{D}}_4$ is not very robust. Notice also that in Figures 10 and 13 the contour lines are unsymmetric at the corners. The operator $\mathbf{D}_1^- \mathbf{D}_1^+ \Sigma \mathbf{D}_2$ does not have this behavior.

The convergence rate of the operator $\mathbf{D}_1^- \Sigma \mathbf{D}_3^+$ is the highest, Figures 6 and 7. Note the significant change of the convergence rate for the operator $\tilde{\mathbf{D}}_4$ for the irrotational flow, and for the operators \mathbf{D}_4 and $\tilde{\mathbf{D}}_4$ for the perturbed flow. The change in convergence rate occurs after about 3,000 iterations in the first case, and about 1,500 iterations in the second case. There is also a decrease in the rate of convergence of the operator $\mathbf{D}_1^- \Sigma \mathbf{D}_3^+$ for irrotational flows at about 1,500 iterations. The convergence rate decreases by almost a factor of two. The convergence properties are summarized in Table 3. The residual at

step n is computed as

$$\frac{\|\rho^n - \rho^{n-1}\|_2}{\|\rho^n\|_2},$$

Dissipation operator	Vorticity at inflow boundary	Entropy S_{\min}	Entropy S_{\max}
$\tilde{\mathbf{D}}_4$	No	43.64	57.57
	Yes	43.56	57.68
$\bar{\mathbf{D}}_4$	No	46.67	46.86
	Yes	46.62	46.74
\mathbf{D}_4	No	46.68	46.78
	Yes	46.58	46.73
$\mathbf{D}_1^- \Sigma \mathbf{D}_3^+$	No	46.76	46.94
	Yes	46.73	46.84

Table 2: Entropy at Outflow Boundary

Dissipation operator	Vorticity at inflow boundary	Number of iterations	Residual
$\tilde{\mathbf{D}}_4$	No	3900	5.8E-6
	Yes	3900	6.8E-6
$\bar{\mathbf{D}}_4$	No	5800	6.6E-6
	Yes	5400	6.6E-6
\mathbf{D}_4	No	3900	5.8E-6
	Yes	5400	6.9E-6
$\mathbf{D}_1^- \Sigma \mathbf{D}_3^+$	No	3400	6.5E-6
	Yes	2800	6.7E-6

Table 3: Number of Iterations for the Dissipation Operators

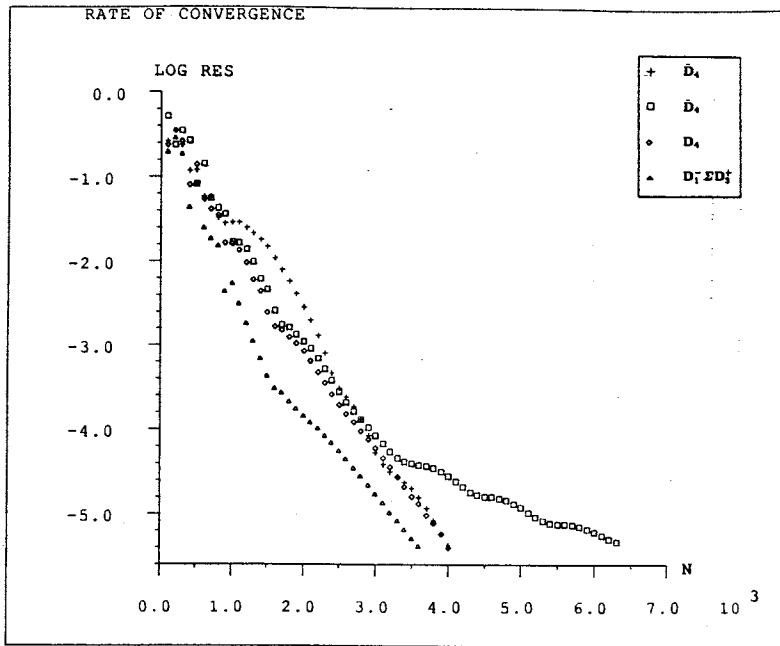


Figure 6: Rate of Convergence for the Different Dissipation Operators, Irrotational Inflow

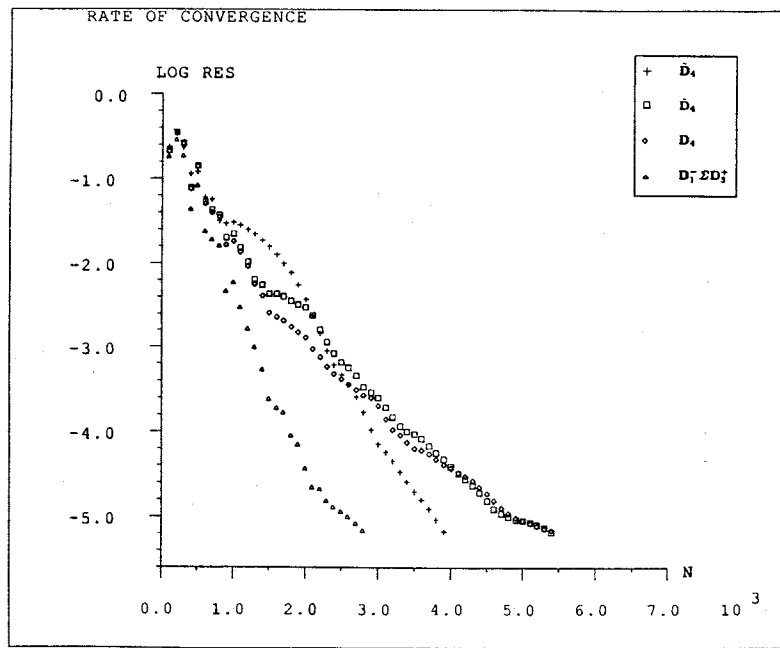


Figure 7: Rate of Convergence for the Different Dissipation Operators, Weakly Rotational Inflow

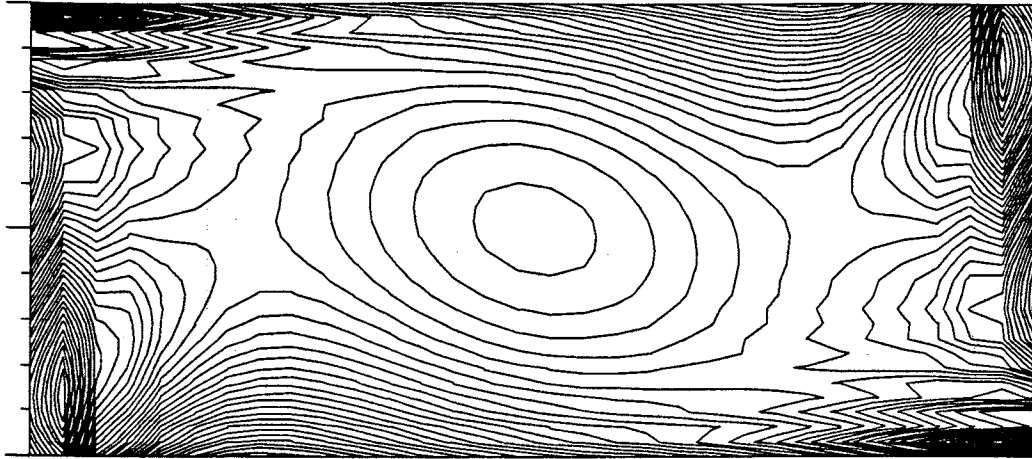


Figure 8: Contour Lines of w -component at Outflow, Operator \bar{D}_4 , Irrotational Inflow

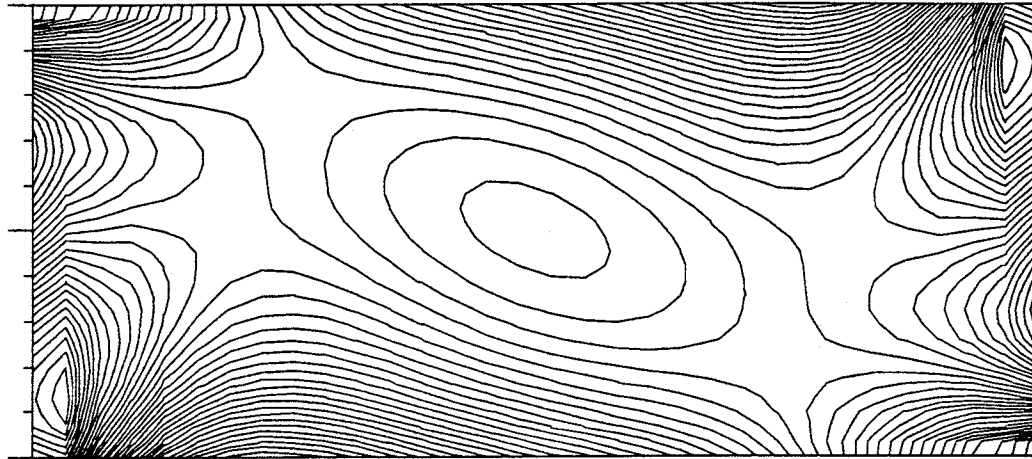


Figure 9: Contour Lines of w -component at Outflow, Operator D_4 , Irrotational Inflow

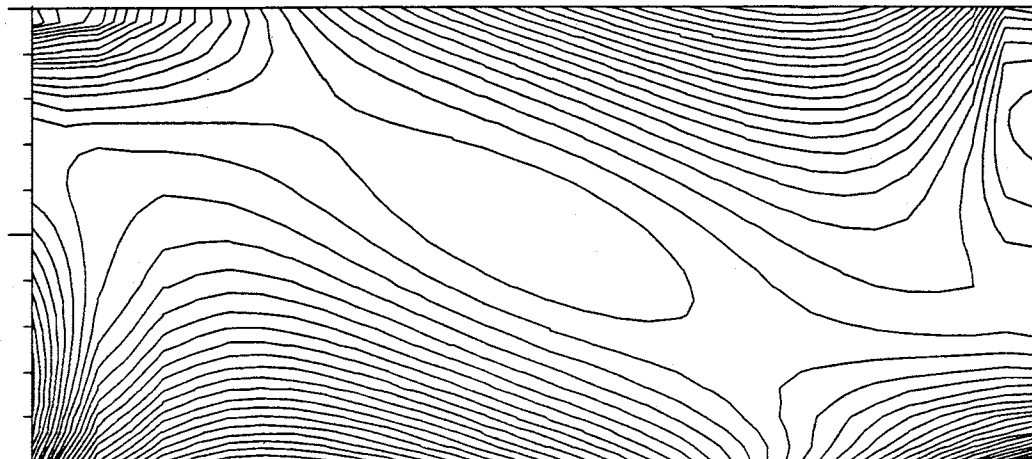


Figure 10: Contour Lines of w -component at Outflow, Operator $\bar{D}_1 \Sigma D_3^\dagger$, Irrotational Inflow

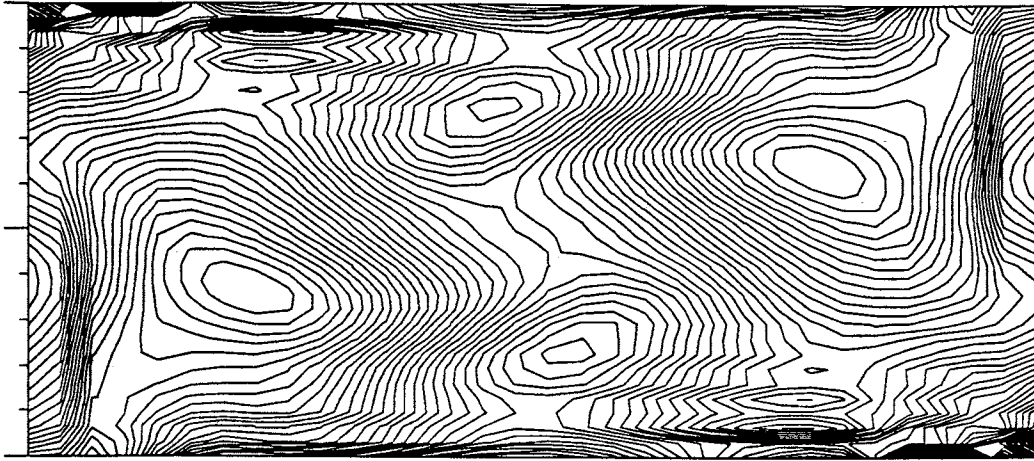


Figure 11: Contour Lines of w -component at Outflow, Operator \bar{D}_4 , Weakly Rotational Inflow

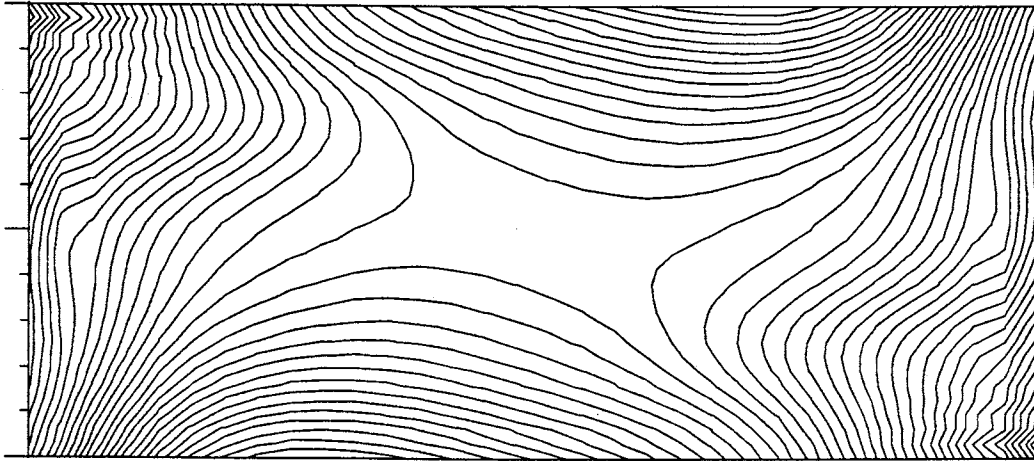


Figure 12: Contour Lines of w -component at Outflow, Operator D_4 , Weakly Rotational Inflow

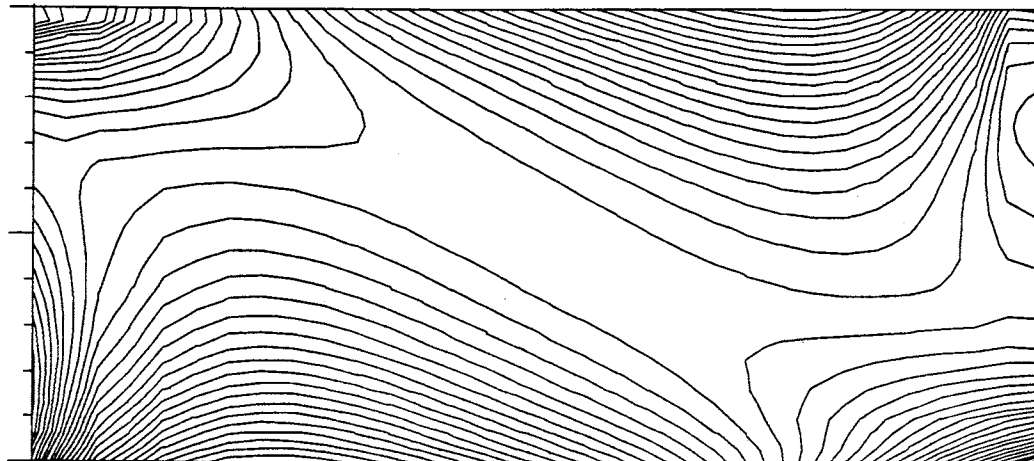


Figure 13: Contour Lines of w -component at Outflow, Operator $D_1^- \Sigma D_3^+$, Weakly Rotational Inflow

5 Summary and Conclusions

We have shown that the non-conservative dissipation operator defined by (66) (see also [8]) gives rise to a significant growth in entropy close to the solid walls of the channel, and that the conservative operators do not have this behavior. We have also shown that factorization of the dissipation operator proposed by Eriksson [4] as $\mathbf{D}_1^- \Sigma \mathbf{D}_3^+$ results in a higher rate of convergence than the unfactored operator, both for irrotational and perturbed inflows. The number of iterations for this operator is approximately 90% of those for the dissipation operator defined by (66) in the irrotational case, and approximately 70% in the perturbed case. The stability of the different operators is not the same. The operator $\mathbf{D}_1^- \Sigma \mathbf{D}_3^+$ appears to be most stable, whereas the operator $\bar{\mathbf{D}}_4$ does not seem to be robust.

The finite difference, explicit time stepping algorithm, parallelizes easily and perfectly. A performance of 135 Mflops/s was obtained on a 8,192 processor Connection Machine system model CM-2. The demonstrated performance for a fully configured system of 65,536 processors is 1.1 Gflops/s.

Acknowledgement

Many thanks are due Bertil Gustafsson for valuable suggestions and critique throughout the project, and for many comments on the manuscript. The first implementation of the Euler and Navier-Stokes solvers was made in Release 4 of the Connection Machine software. Porting of the program to Release 5 was made by Louis Howell and David Serafini of Thinking Machines Corporation.

References

- [1] R. Courant and K. O. Friedrichs. *Supersonic Flow and Shock Waves*, volume I of *Pure and Applied Mathematics*. Interscience Publishers, Inc., New York, 1948.
- [2] G. Dahlquist, Å. Björck, and N. Anderson. *Numerical Methods*. Series in Automatic Computation. Prentice Hall, Inc., Englewood Cliffs, NJ, 1974.
- [3] Rickard Enander and Johan Sowa. Numerical simulation of fluid flow in a twisted channel. Technical Report 88-01, Department of Scientific Computing, Uppsala University, 1988.
- [4] L. E. Eriksson. Boundary conditions for artificial dissipation operators. Technical Report FFA TN 1984-53, The Aeronautical Research Institute of Sweden, Aerodynamics Department, Stockholm, Sweden, 1984.
- [5] A. Jameson, W. Schmidt, and E. Turkel. Numerical solutions of the Euler equations by finite volume methods using Runge-Kutta time-stepping schemes. *AIAA Paper*, 81-1259, 1981.
- [6] S. Lennart Johnsson. Future high performance computation: The megaflop per dollar alternative. Technical Report YALEU/DCS/RR-360, Dept. of Computer Science, Yale University, January 1985.
- [7] Pelle Olsson and S. Lennart Johnsson. A dataparallel implementation of explicit methods for the three-dimensional compressible Navier-Stokes equations. Technical Report CS-89/4, Thinking Machines Corp., February 1989.
- [8] Thomas E Pulliam. Artificial dissipation models for the Euler equations. *AIAA*, 24(12), December 1986.
- [9] R.F. Warming, Richard M. Beam, and B.J. Hyett. Diagonalization and simultaneous symmetrization of the gas-dynamic matrices. *Mathematics of Computation*, 29(132), October 1975.